Comparison of Alzheimer Aβ(1–40) and Aβ(1–42) amyloid fibrils reveals similar protofilament structures

Matthias Schmidt[a,b,c], Carsten Sachse[a,b,1], Walter Richter[d], Chen Xu[a], Marcus Fändrich[b], and Nikolaus Grigorieff[a,c,2]

[a]Rosenstiel Basic Medical Sciences Research Center and [c]Howard Hughes Medical Institute, Brandeis University, MS 029, Waltham, MA 02454-9110; [b]Max-Planck Research Unit for Enzymology of Protein Folding and Martin-Luther University Halle-Wittenberg, Weinbergweg 22, 01620 Halle (Saale), Germany; and [d]Elektronenmikroskopisches Zentrum, Friedrich-Schiller-Universität Jena, Ziegelmühlenweg 1, 07740 Jena, Germany

Edited by David Baker, University of Washington, Seattle, WA, and approved September 16, 2009 (received for review May 6, 2009)

We performed mass-per-length (MPL) measurements and electron cryomicroscopy (cryo-EM) with 3D reconstruction on an Aβ(1–42) amyloid fibril morphology formed under physiological pH conditions. The data show that the examined Aβ(1–42) fibril morphology has only one protofilament, although two protofilaments were observed with a previously studied Aβ(1–40) fibril. The latter fibril was resolved at 8 Å resolution showing pairs of β-sheets at the cores of the two protofilaments making up a fibril. Detailed comparison of the Aβ(1–42) and Aβ(1–40) fibril structures reveals that they share an axial twofold symmetry and a similar protofilament structure. Furthermore, the MPL data indicate that the protofilaments of the examined Aβ(1–40) and Aβ(1–42) fibrils have the same number of Aβ molecules per cross-β repeat. Based on this data and the previously studied Aβ(1–40) fibril structure, we describe a model for the arrangement of peptides within the Aβ(1–42) fibril.

Alzheimer's disease | electron microscopy | prion | protein folding

Amyloid fibrils are fibrillar polypeptide aggregates that consist of a cross-β structure (1, 2). They accumulate inside the human body in the course of aging and are associated with several debilitating conditions such as Alzheimer disease (AD) (1, 2). AD amyloid fibrils are formed from Aβ peptide, which occurs in isoforms of different length. The 40-residue peptide Aβ(1–40) represents the most abundant Aβ isoform in the brain (3), while the 42-residue Aβ(1–42) shows a significant increase with certain forms of AD (4). Aβ amyloid fibrils have been analyzed with various biophysical and biochemical techniques, such as solid-state NMR (NMR) spectroscopy, solution state NMR spectroscopy coupled with hydrogen/deuterium exchange, or mutagenesis (5–8). These analyses have provided a wealth of information about specific structural details of the peptide in the fibril, for example dihedral torsional angles, protection factors or distances between specific atoms. Atomic models for Aβ peptides and their assembly in different amyloid fibrils have been constructed based on such data (6, 8–10) but these models have not been confirmed by more direct 3D imaging methods.

A hallmark of Aβ amyloid fibrils is their substantial polymorphism (11–14). We have recently shown by transmission electron cryomicroscopy (cryo-EM) and 3D reconstruction that Aβ(1–40) fibrils form a range of morphologies with almost continuously altering structural properties (13). Despite their different morphologies, the cross-sectional areas of the reconstructed fibrils were similar. The study suggested that the observed polymorphism may be the result of different packing of protofilaments that have the same basic structure. To obtain an image of a fibril at higher resolution, we established growth conditions that promote a specific Aβ(1–40) fibril morphology (15) and selected fibrils with this morphology from electron micrographs for further processing. Using newly developed image processing tools (16), we obtained a 3D image at 8 Å resolution from images of 188 fibrils (17). The image reconstruction revealed a fibril consisting of two protofilaments, and it resolved pairs of cross-β sheets at the core of each protofilament. The observed cross-β sheet pairing resembled the recently proposed steric zipper model for amyloid spines (18) and suggested a protofilament core formed by two oppositely directed Aβ peptides. Mass-per-length (MPL) measurements further revealed that the fibril contains five peptides per cross-β repeat, or 2.5 peptides per repeat in one protofilament. The inconsistency between the 2.5 peptides per repeat indicated by the MPL measurements, and the two peptides per repeat implied by the paired β sheet model, was explained by additional peptide associated with the cross-β core of the fibril. The presence of additional peptide was also suggested by additional weak density visible at the periphery of the fibril core. The weak density is consistent with a more irregular peptide arrangement averaging 0.5 peptides per cross-β repeat, contrasting with the regular periodic structure of the fibril core.

In the present study, the structure of an Aβ(1–42) fibril morphology formed under physiologically relevant pH conditions is compared with two observed Aβ(1–40) fibril morphologies. Using scanning transmission electron microscopy (STEM), we show that all three morphologies have the same non-integer number of ≈2.5 peptides per cross-β repeat per protofilament. Furthermore, we use cryo-EM to generate a 3D reconstruction of the Aβ(1–42) fibril morphology and compare it to reconstructions of the Aβ(1–40) fibril morphologies. Although the reconstructed morphologies show significant differences, there is also evidence for common structural principles among different Aβ fibril morphologies.

Results

Amyloid characteristics of the analyzed Aβ(1–42) fibril. The analyzed Aβ(1–42) fibrils were obtained by in vitro incubation of 1 mg/mL Aβ(1–42) peptide in 50 mM Tris·HCl buffer, pH 7.4. After incubation for at least two days, the sample contained large quantities of fibrils, as confirmed by transmission electron microscopy (TEM) and standard biophysical methods (see *SI Materials and Methods*). Attenuated total reflectance Fourier-transform infrared (ATR-FITR) spectroscopy shows amide I and II maxima centered at 1,628 and 1,551 cm^{-1} (Fig. S1*A*). The recorded position of the amide I maximum is characteristic for the β-sheet structure of amyloid fibrils (19). Fibril samples also

Author contributions: M.F. and N.G. designed research; M.S., C.S., W.R., and C.X. performed research; W.R. contributed new reagents/analytic tools; M.S., C.S., M.F., and N.G. analyzed data; and M.S., M.F., and N.G. wrote the paper.

The authors declare no conflict of interest.

This article is a PNAS Direct Submission.

Freely available online through the PNAS open access option.

Data deposition: Density maps have been deposited in the Macromolecular Structure Database of the European Bioinformatics Institute {accession codes EMD-1649 [twofold symmetrized Aβ(1–42) fibrils] and EMD-1650 [13-nm Aβ(1–40) fibrils]}.

[1]Present address: MRC Laboratory of Molecular Biology, Protein and Nucleic Acid Chemistry, Hills Road, Cambridge CB2 0QH, United Kingdom.

[2]To whom correspondence may be addressed. E-mail: fandrich@enzyme-halle.mpg.de or niko@brandeis.edu.

This article contains supporting information online at www.pnas.org/cgi/content/full/0905007106/DCSupplemental.

showed strong interactions with the amyloid-specific dyes Congo red or Thioflavin T (Fig. S1 *B–D*). Congo red bound fibrils produced apple-green birefringence when viewed in a polarizing microscope (Fig. S1 *B* and *C*). X-ray diffraction measurements of Aβ(1–42) fibrils gave rise to Bragg spacings at 4.67 ± 0.04 Å and 9.7 ± 0.3 Å (Fig. S2). Spacings at these positions represent typical characteristics of amyloid structures (20). The 4.7 Å reflection is termed "main chain" spacing and represents the distance of hydrogen bonded β-strands, while the 10 Å "side chain" spacing represents the packing distance of laminated β-sheet layers. Taken together, these data establish the amyloid-like characteristics of the Aβ(1–42) fibrils used in the present analysis.

Morphological Homogeneity of the Analyzed Fibril Sample. Cryo-EM shows that the analyzed sample contained large quantities of well-separated, unbranched fibrils of highly periodic structure. Almost all of the fibrils present regularly spaced cross-overs, indicative of a twisted fibril structure (Fig. 1*A*). Unidirectional platinum shadowing, coupled with TEM analysis, shows that the fibrils have a left-handed twist (Fig. S3). A left-handed helical twist is also found with many Aβ(1–40) fibrils (12, 13, 15). Measurement of the cross-over distances of 41 fibrils yields a relatively narrow distribution (Fig. 1*B* and Table 1). In addition, the fibrils are relatively similar in fibril width (Fig. 1*C* and Table 1). The low variation of these measurements indicates a high morphological homogeneity of the analyzed fibril sample. We compared this Aβ(1–42) fibril morphology with two Aβ(1–40) fibril morphologies present in a previously studied sample (15). These include the most frequently observed morphology with a fibril width between cross-overs of ≈20 nm (henceforth referred to as the 20-nm Aβ(1–40) morphology), and an infrequently observed morphology with a fibril width between cross-overs of ≈13 nm (referred to here as the 13-nm Aβ(1–40) morphology) (15). The standard deviations of the histogram distributions and errors are given in Table 1.

STEM Analysis. We performed STEM analysis combined with MPL measurements on all three fibril morphologies (Fig. 2). All MPL data were calibrated using Tobacco Mosaic Virus (TMV) and the standard deviations of the Gaussians fitted to the histograms closely match those of the MPL data for TMV (Fig. S4 *A* and *B*) (17). Therefore, the histogram distribution represents mainly an intrinsic error of the MPL measurements, and not a variability of fibril mass. The errors of the peak positions of the Gaussians fitted to the histograms are 0.4% or less in all cases (Table 1). For the Aβ(1–42) fibril, we obtained an average MPL value of 23.5 ± 0.1 kDa/nm. Using the theoretical molecular mass of an Aβ(1–42) molecule (4514 Da), the recorded MPL value translates into 2.44 Aβ(1–42) molecules for each 4.7 Å repeat of the fibril. Previous MPL analysis of the significantly wider 20-nm Aβ(1–40) fibril (17) yielded approximately twice this value, i.e., an average of 4.97 Aβ(1–40) molecules (4330 Da) or ≈2.5 Aβ molecules per cross-β repeat within one Aβ(1–40) protofilament. Virtually the same result of 4.91 molecules per cross-β repeat was found for the 13-nm Aβ(1–40) fibril. Hence, all analyzed Aβ(1–40) fibrils show a basic number of ≈5 peptide per cross-β repeat, while the presently reconstructed Aβ(1–42) fibril contains only half this number of peptides.

Three-Dimensional Reconstruction. We calculated a 3D reconstruction of the Aβ(1–42) fibril as described in ref. 17 using 14 fibril images from our cryo-EM dataset (Fig. 3 *A* and *B*). These were segmented into 572 overlapping segments for further processing (segment length: 158.4 × 158.4 nm). We selected fibrils with a minimal length of 300 nm and the smallest possible curvature. Furthermore, the selected fibrils included cross-over distances between 103 nm and 117 nm that were close to the distribution

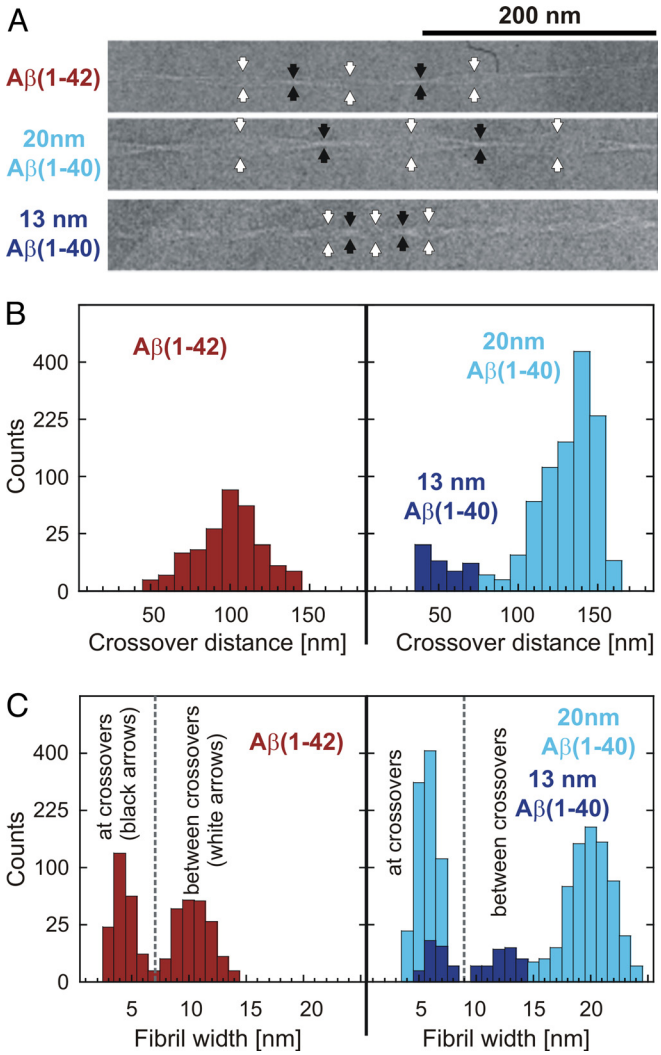

Fig. 1. Fibril structure and structural homogeneity of the analyzed sample. (*A*) Cryo-EM images of Aβ(1–42), 20-nm Aβ(1–40) and 13-nm Aβ(1–40) fibrils. cross-overs and the widest points between cross-overs are indicated by black and white arrow heads, respectively. (*B*) Distribution of cross-over distances and (*C*) fibril widths (measured at the cross-overs and the widest points between cross-overs) for all three types of fibrils. The counts are plotted on a non-linear (square root) scale to make small counts more visible. Measurement results are provided in Table 1.

maximum of 108 nm (Fig. 1*B*). This represents ≈34% of the imaged fibrils. The resolution of the reconstruction was ≈15 Å based on the 0.5 Fourier shell correlation (FSC) criterion (21) (Fig. S5*A* and Table 2). Projections of the 3D density map show good correspondence with the raw cryo-EM data (Fig. S5*B*). The observed match indicates that the obtained reconstruction is consistent with the raw data.

The reconstructed fibril is clearly polar. Fibril dimensions were measured using contour levels 1.5× the estimated standard error of the map above background (bold lines in Fig. 3). The Aβ(1–42) fibril cross-section exhibits dimensions of ≈4 × 11 nm (Fig. 3*B*) and reflects the twofold symmetry imposed during reconstruction. The assumption of a twofold symmetry is based on a 3D reconstruction without imposed symmetry, which shows a similar cross-section and overall fibril topology (Fig. S6*A*). A twofold symmetry is consistent with most other amyloid fibril morphologies (13, 16, 22, 23). Hereafter, we will refer only to the twofold symmetrized reconstruction.

Table 1. Statistics of the histogram distributions shown in Fig. 1 and 2

Statistic	Aβ(1–42)	20 nm Aβ(1–40)	13 nm Aβ(1–40)
Crossover distance, nm (Fig. 1)			
No. of measurements	213	1036	31
Histogram STD	14.6	11.4	13.6
Average	100.8	136.9	53.4
Error of the average	1.0	0.4	2.4
Width at crossover, nm (Fig. 1)			
No. of measurements	213	850	26
Histogram STD	0.69	0.73	0.71
Average	4.23	5.73	6.57
Error of the average	0.05	0.02	0.13
Width between crossover, nm (Fig. 1)			
No. of measurements	180	686	25
Histogram STD	1.19	1.45	1.41
Average	10.36	20.02	13.23
Error of the average	0.08	0.06	0.26
MPL measurements, kDa/nm(Fig. 2)			
No. of measurements	2674	9424	734
STD of Gaussian fit	4.97	5.39	4.74
Peak of Gaussian fit	23.47	45.77	45.23
Error of peak position	0.10	0.06	0.17
Molecules per 4.7 Å repeat	2.44	4.97	4.91

For each histogram, an average and error of the average of the distribution are calculated. In the case of fibril crossover distances and widths (Fig. 1), an average is calculated as the sum of all measurements contributing to a histogram divided by the number of measurements. The error of the average is calculated as the standard deviation of the histogram divided by the square root of the number of measurements contributing to the histogram. For the TMV-calibrated MPL measurements (Fig. 2), the average was taken to be the peak of the Gaussian fit for each histogram. The error of this value is calculated as the standard deviation of the Gaussian divided by the square root of the number of measurements.

The cross-section of the Aβ(1–42) fibril image has an approximate area of 44 nm^2 (Fig. 3*B*), which is approximately half the area measured for the corresponding cross-section of the 20-nm Aβ(1–40) fibril image (90 nm^2, Fig. 3*C*). Using the MPL measurements and an average protein density of 810 Da/nm^3 (24), cross-sectional areas of 30 nm^2 and 58 nm^2 are calculated for the Aβ(1–42) and 20-nm Aβ(1–40) fibrils, respectively. These values are smaller than those measured using the density maps, presumably due to loose packing and variable conformation of some portions of the peptide. The cross-section of the Aβ(1–42) fibril image can be divided into three regions, one central region termed C_{42} and two peripheral regions termed P_{42}. The central region is concentric with the main fibril axis. It presents an elongated shape of ≈4 × 5 nm, and it is sandwiched between the two P_{42} regions. The latter occur at outer radial positions and present a more diffuse density. Furthermore, the C_{42} substructure reveals two regions of higher density, while only a single high density feature can be discerned in each P_{42} region.

We also processed two of the cryo-EM images of the rarely observed 13-nm Aβ(1–40) fibril and calculated a reconstruction (Fig. 3 *A* and *D*) at ≈23 Å resolution (Fig. S5*A* and Table 2). Projections of this structure correspond well with the raw images (Fig. S5*C*), and they also indicate that this fibril is polar. The cross-section of the twofold symmetrized fibril reconstruction has dimensions of ≈6 × 13 nm and an area of ≈77 nm^2. It shares features with the non-symmetrized reconstruction (Fig. S6*B*) but the correspondence is not as good as for the Aβ(1–42) fibril due to substantial noise resulting from the small size of the dataset.

Discussion

When interpreting 3D reconstructions of amyloid fibrils in terms of possible peptide folds and packing arrangements, one of the strongest constraints is provided by the MPL measurements. The structure of the 20-nm Aβ(1–40) amyloid fibril (17) consists of two protofilaments, and MPL measurements indicate that it contains 4.97 peptides per 4.7 Å cross-β repeat. The MPL measurements presented here for the Aβ(1–42) and 13-nm Aβ(1–40) fibrils indicate 2.44 and 4.91 peptides per cross-β repeat, respectively. This suggests that the number of protofilaments for these two fibril morphologies is 1 and 2. This interpretation is further supported by a comparison of the cross-sectional structures of these fibrils with that of the 20-nm Aβ(1–40) fibril.

Although the 20-nm Aβ(1–40) fibril structure differs significantly from the presently described Aβ(1–42) fibril structure, we note important similarities between individual Aβ(1–40) protofilaments and the Aβ(1–42) fibril. The most significant similarity is the number of Aβ molecules per cross-β repeat (see above). Furthermore, the cross-sectional size of one Aβ(1–40) protofilament measures 4 × 11 nm (Fig. 3*C*), which is the same for the Aβ(1–42) fibril (Fig. 3*B*). A more detailed comparison of features of the Aβ(1–42) fibril and one Aβ(1–40) protofilament can be made by considering different density regions in both structures. Similar to the division of the Aβ(1–42) fibril (Fig. 3*B*), we name the two peripheral regions of one Aβ(1–40) protofilament $P_{40}{}^{a}$ and $P_{40}{}^{b}$, and the cross-β core C_{40} (Fig. 3*C*). C_{42} and C_{40} have the same overall dimensions (4 × 5 nm). Furthermore, the local pseudo twofold symmetry of C_{40} corresponds to the twofold symmetry of C_{42}. Unlike in the case of Aβ(1–40), however, the two peripheral regions of Aβ(1–42) share the same environment and their diffuse density suggests disorder in this part of the structure. The two P_{42} regions resemble, by their solvent exposure and cross-sectional structure,

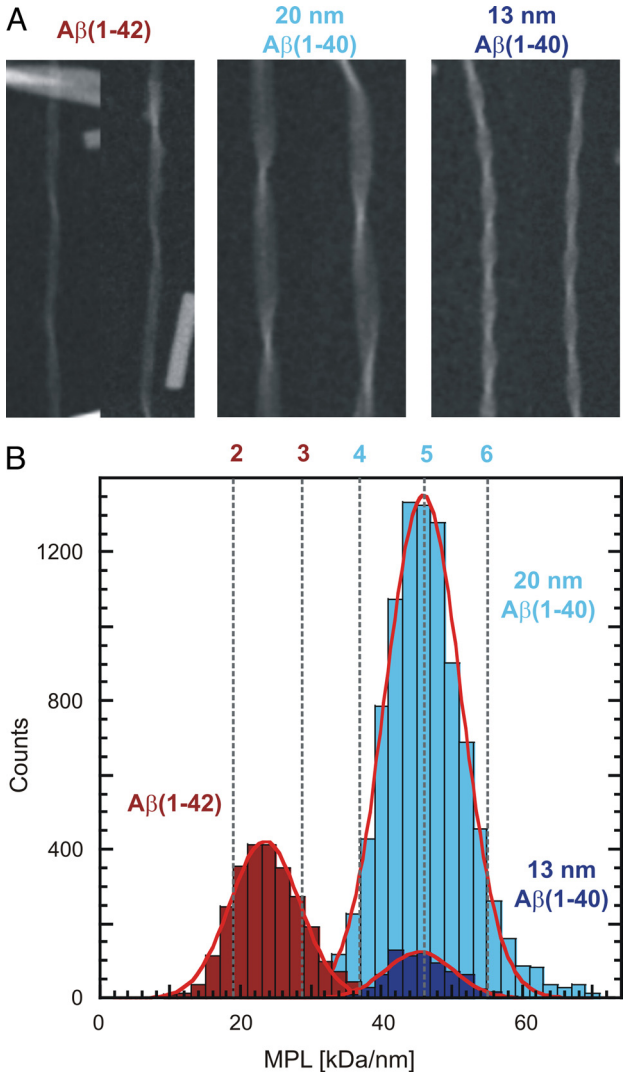

Fig. 2. STEM analysis of Aβ(1–40) and Aβ(1–42) fibrils. (*A*) STEM images of Aβ(1–42), 20-nm Aβ(1–40) and 13-nm Aβ(1–40) fibrils. (*B*) MPL measurements for all three fibril types. Measurement results are provided in Table 1. The standard deviation of the distribution of all histograms is the same standard deviation that is also found for TMV, which was used to calibrate the MPL measurements (Fig. S4). STEM data for the 20-nm Aβ(1–40) was taken from ref (17). The red and blue numbers above the histograms refer to number of Aβ molecules per 4.7 Å repeat, assuming Aβ(1–42) and Aβ(1–40) molecules, respectively.

the properties of $P_{40}{}^{b}$; they all display a diffuse density (Fig. 3 *B* and *C*).

These comparisons provide further evidence that the analyzed Aβ(1–42) fibril consists of one protofilament, and that the C_{42} region may harbor two juxtaposed β-sheets (Fig. 3*B*), similar to the core regions of the Aβ(1–40) protofilaments (Fig. 3*C*). The analogy to Aβ(1–40) further implies that the peptide N termini make up the P_{42} regions, while the peptide C termini form the fibril core (C_{42}). Consistent with this proposal, we find that the C_{42} substructure is comprised of two packed density cores that are separated from each other by a central lower density. However, a direct observation of this proposed packing arrangement will require higher resolution.

The MPL measurements indicating a non-integer number of ≈2.5 peptides per cross-β repeat in one protofilament are intriguing because they are incompatible with a fibril structure consisting only of peptides forming parallel in-register β-sheets. Non-integer numbers of peptides per cross-β repeat were also obtained for other amyloid fibrils (25). This lends support to our MPL measurements. Furthermore, several other MPL measurements of Aβ fibrils have been published that report values with substantial deviations from those expected for an integer number of peptides per cross-β repeat (12, 26, 27). In these studies, the datasets were smaller than those used here, and the deviations were attributed to measurement error. In other cases, the fibril populations were too heterogeneous to yield MPL measurements that could be fitted by a single Gaussian (9, 12, 26, 28). The error analysis (Table 1) shows that in our study the deviation of the number of peptides per cross-β repeat from an integer is not due to a random measurement error. Furthermore, our fibril populations are sufficiently homogeneous to yield MPL data that can be fitted by single Gaussians with standard deviations comparable to that for TMV particles included with the amyloid fibrils.

It is possible that some Aβ molecules attach peripherally to the fibril with an average spacing of two cross-β repeats. Such additional molecules, decorating the actual fibril core, would be consistent with some low-density features seen with the 8 Å Aβ(1–40) fibril structure (17). Such disordered peptide may be difficult to detect by spectroscopic methods. Alternatively, instead of a loose peripheral association, peripheral Aβ peptides could swap domains with peptides from the fibril core with a frequency that averages to ≈0.5 peptides per cross-β repeat. Systematic errors can affect the observed MPL data. With the Aβ(1–42) fibrils, we regularly observe a systematic increase of the measured MPL values of ≈15% at the positions of the cross-overs compared with measurements in between cross-overs. This leads to a 2% increase of the averaged MPL value for a typical fibril, compared with an average that excludes cross-overs. It is possible that the observed increase in mass is due to residual buffer that is not removed during freeze-drying, or due to denatured peptide that accumulates at the cross-overs. The average mass increase at the 13-nm and 20-nm Aβ(1–40) fibril cross-overs is <5%. The smaller value might be the result of the different morphologies or the different buffers used with the Aβ(1–42) (50 mM Tris/HCl at pH 7.4) and Aβ(1–40) fibrils [50 mM sodium borate at pH 8.7 (17)].

The 13-nm Aβ(1–40) fibril structure corresponds closely with one of the morphologies described previously (fibril 2 in ref. 13). However, due to the small size of the dataset, the resolution of the reconstruction is lower compared with the other two structures. Therefore, the interpretation of the density is less clear. Based on the similar cross-sectional area of the previously studied fibril morphologies (77 nm^2 for the 13-nm Aβ(1–40) fibril versus 90 nm^2 for the 20-nm Aβ(1–40) fibril), this fibril was also thought to consist of two protofilaments, each containing a pair of cross-β sheets (13). The difference of 13 nm^2 between the two cross-sectional areas may be due to the different quality of the two reconstructions, differences in the packing of the protofilaments, or different packing of the Aβ peptide within them. The MPL measurements further support the similarity between the 13-nm and 20-nm Aβ(1–40) fibrils.

The results obtained for all three fibril structures presented here suggest that they share the same fundamental protofilament structure, in agreement with earlier work using electron paramagnetic resonance (29). This would place the peptide N termini at the periphery of a protofilament, while the C termini would form its core. The different morphologies would, therefore, arise mainly from the different packing and number of protofilaments. This model does not exclude the possibility of variable side chain interactions between molecules within protofilaments, or differences in the structure and ordering of the N terminus. However, protofilaments would have an antiparallel arrangement of peptides in common that form pairs of parallel-stranded cross-β sheets.

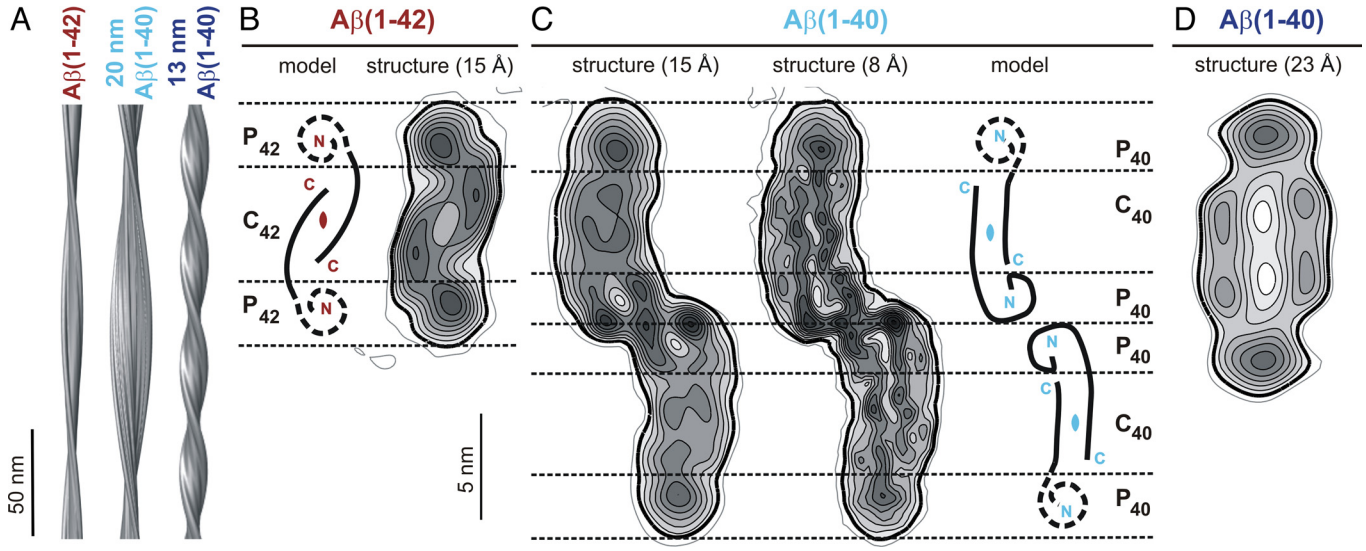

Fig. 3. Reconstructed densities of Aβ(1–40) and Aβ(1–42) fibrils. (*A*) Side views of reconstructions of Aβ(1–42) and Aβ(1–40) fibrils. (*B*) Density map of the fibril Aβ(1–42) cross-sections (*Right*) and possible peptide placement (*Left*), guided by previous interpretations shown in *C*. The cross-sectional area is ≈44 nm^2. (*C*) Cross-sections of the 20-nm Aβ(1–40) fibril density map filtered at 15 Å (*Left*) and 8 Å resolution (*Center*) (17). The cross-sectional area is ≈90 nm^2. (*Right*) Interpretation of the 20-nm Aβ(1–40) fibril cross-section (17). (*D*) Cross-section of the 13-nm Aβ(1–40) fibril density map. The cross-sectional area is ≈77 nm^2. Contours represent density levels of multiples of 1.5× the estimated standard errors for each map. The first contour represents the average density of the background in each case. The bold contours indicate the contours used for the measurements of dimensions and area.

In addition to the Aβ fibrils analyzed here, numerous other types of Aβ(1–40) or Aβ(1–42) fibril morphologies are reported in refs. 6, 12, and 13, including some with MPL-values that do not correspond to integer numbers of peptides per cross-β repeat (12). Hence the present analysis addresses only a small part of the conformational diversity of Aβ fibrils. Recently, the 3D reconstruction of another Aβ(1–42) amyloid fibril morphology has been reported (30). Although this Aβ(1–42) fibril was also interpreted by an arrangement of two peptides in the cross-section, this interpretation was not complemented by MPL measurements. Moreover, the fibril structure differs substantially from the one described here. The reported density shows a tubular arrangement, encompassing a central and putatively water-filled hole of 4-nm diameter, and the wall surrounding the hollow core is formed by a peptide layer of 2-nm thickness. No such architecture has been observed for any other Aβ fibril morphology. The hollow fibrils were obtained by incubation of 100 μM Aβ(1–42) in 2% dimethylsulfoxide and 10 mM HCl for at least one month (37 °C). Because the authors report a pH value of ≈2 (30), these strongly acidic and very long incubation conditions differ substantially from those used here for Aβ(1–42) fibrils or those used for Aβ(1–40) fibrils. Incubation conditions are known to affect the fibril structure (31). Therefore, the presence of hollow Aβ(1–42) fibrils under physiological conditions remains to be established.

Table 2. Image processing statistics

Statistic	Aβ(1–42)	13 nm Aβ(1–40)
Pixel size on the specimen, Å	4.8	4.8
Resolution at FSC = 0.5, Å	15	23
Total length of non-overlapping segments, nm	4806	857
No. of fibrils	14	2
No. of segments	572	108
Segment size, nm	158.4	158.4
Size of 3D reconstruction, nm	77.7	77.7
Segment step size, nm	6.5	6.5
Crossover distance, nm	108	49
Repeat distance, nm	0.47	0.47
Fibril width, nm	10	13
Cross-sectional area, nm^2	44	77

Several biochemical and biophysical analyses led to the proposal of atomic models for fibrillar Aβ(1–40) or Aβ(1–42) peptides (6, 8, 10, 32–34). However, these models were not uniquely determined by the experimental data. A remarkable result of the 3D reconstructions reported here is that none of the currently existing models is able to explain all structural features encountered here. These data show that the structures of Aβ(1–40) and Aβ(1–42) fibrils are evidently more complex than has been anticipated by previous studies. Specifically, fibril morphologies with different cross-sectional architecture cannot be represented by a single atomic model. This is consistent with NMR data indicating the presence of several different peptide conformations associated with different fibril morphologies (6, 10). Furthermore, a central observation emerging from our studies, as well as from others (28), is the existence of multiple peptide folds within a single fibril morphology. In particular, the morphology of the Aβ(1–40) fibril determined at 8 Å resolution (17) suggests two peptides that share a common structure at their C terminus, but different structures at their N terminus. The MPL measurements indicating non-integer multiples of peptides per cross-β repeat may be another indication of different peptide conformations present within a single fibril. Further structural data, specifically cryo-EM reconstructions at higher resolution, will be required to resolve the true underlying atomic structures of fibrils or other aggregates formed from Alzheimer Aβ peptides. Such data would represent a sensible starting point for in-depth structural assessment of the amyloid fold by molecular dynamics simulations or docking studies using potential amyloid ligands.

Materials and Methods

Fibril Preparation. Synthetic Aβ(1–42) peptide was obtained from BACHEM (lot no. 0572194; the purity was at least 93%, measured by analytical HPLC/reverse phase chromatography). Fibrils were formed at 1 mg/mL concentration by incubation in 50 mM Tris/HCl (pH 7.4), at room temperature for a

minimum of 2 days. Other lots of Aβ(1–42) from BACHEM sometimes show a higher structural heterogeneity of fibril forms.

Electron Microscopy. CEM samples were prepared as described in ref. 15. Vitrified specimens were imaged in a Tecnai F30 microscope at 300 kV, with a magnification of 59,000 and low-dose conditions and a temperature of −180 °C. Micrographs were recorded at an underfocus of 1.75, 2.0 and 2.5 μm on Kodak SO 163 film.

Scanning Transmission Electron Microscopy (STEM). Experiments were performed at the Brookhaven National Laboratory. The preparation and image acquisition conditions are described in ref. 35. Dark-field images with pixel sizes of 1 nm and 2 nm were analyzed using the computer program PCMASS29 (35) with the filament trace option and a mask of 40-nm length and appropriate width. The MPL measurements were calibrated with Tobacco Mosaic Virus (TMV) for each individual image as described in ref. 25, and a cross-β repeat of 4.7 Å for all fibril morphologies was assumed.

Image Processing. Micrographs were selected for micrograph and fibril quality. Fibril quality was defined by length and straightness. Cross-over distances of appropriate Aβ(1–42) fibrils were limited to 110 nm $\pm$ 7 nm. The micrographs were digitized using a Zeiss SCAI flatbed scanner with a raster size of 7 μm, resulting in a pixel size of 1.2 Å. A more detailed description is in ref. 16. The cross-over of 14 fibrils were boxed using EMAN's boxer program (36). Boxes along the fibril were added within 60 nm from each cross-over with 6.5-nm step size. The resulting image stack contained 572 squares of 158.4 $\times$ 158.4 nm. A pixel size of 4.8 Å was used for the reconstruction. For the image processing we used SPIDER (37) and calculated a reconstruction of 77.7 $\times$ 77.7 $\times$ 77.7 nm in size. All studied fibrils appear polar and the image processing procedure (16) includes a test of polarity to ensure correct alignment. The parameters of out-of-plane tilt and helical axis angles were restrained during the alignment in addition to restraints applied to the x-shift and in-plane rotation angle, as described in refs. 16 and 17. The specimen out-of-plane tilt angle was measured by CTFTILT (38). A linear regression was performed based on the views, including cross-overs to predict the angles for the views between the cross-overs while obeying an ideal symmetry. Additional twofold symmetry was assumed by aligning each segment in two possible orientations differing by 180° rotation around the helical axis. For the reconstruction, we imposed helical symmetry with a rotation of 0.78° per repeat for the Aβ(1–42) fibril, and a rotation of 1.73° per repeat for the 13-nm Aβ(1–40) fibril. Table 2 contains details about the image processing. The standard error in the densities of the reconstructions was estimated from the difference between the two reconstructions used to estimate the Fourier shell correlation (FSC) curve as half the standard deviation. For the resolution estimation, the FSC was evaluated in a plane perpendicular to the fibril axis.

ACKNOWLEDGMENTS. We thank J. Wall and M. Simon (Brookhaven National Laboratory, Upton, NY) for performing STEM analysis, C. Parthier for assistance in recording the X-ray diffraction data, and D. Caspar for careful reading of the manuscript and his invaluable comments. This work was supported by a long-term European Molecular Biology Organization postdoctoral fellowship (to C.S.), National Institutes of Health Grant 1 P01 GM-62580 (to N.G.); and grants from Bundesministerium für Bildung und Forschung (BioFuture), Deutsche Forschungsgemeinschaft Grant SFB 610, and the Exzellenznetzwerk Biowissenschaften of Sachsen-Anhalt (to M.F.).

1. Fandrich M (2007) On the structural definition of amyloid fibrils and other polypeptide aggregates. *Cell Mol Life Sci* 64:2066–2078.
2. Chiti F, Dobson CM (2006) Protein misfolding, functional amyloid, and human disease. *Annu Rev Biochem* 75:333–366.
3. Mori H, Takio K, Ogawara M, Selkoe DJ (1992) Mass spectrometry of purified amyloid beta protein in Alzheimer's disease. *J Biol Chem* 267:17082–17086.
4. Naslund J, et al. (1994) Relative abundance of Alzheimer A beta amyloid peptide variants in Alzheimer disease and normal aging. *Proc Natl Acad Sci USA* 91:8378–8382.
5. Kodali R, Wetzel R (2007) Polymorphism in the intermediates and products of amyloid assembly. *Curr Opin Struct Biol* 17:48–57.
6. Luhrs T, et al. (2005) 3D structure of Alzheimer's amyloid-beta(1–42) fibrils. *Proc Natl Acad Sci USA* 102:17342–17347.
7. Makin OS, Serpell LC (2005) Structures for amyloid fibrils. *FEBS J* 272:5950–5961.
8. Petkova AT, et al. (2002) A structural model for Alzheimer's beta-amyloid fibrils based on experimental constraints from solid state NMR. *Proc Natl Acad Sci USA* 99:16742–16747.
9. Paravastu AK, Leapman RD, Yau WM, Tycko R (2008) Molecular structural basis for polymorphism in Alzheimer's beta-amyloid fibrils. *Proc Natl Acad Sci USA* 105:18349–18354.
10. Petkova AT, Yau WM, Tycko R (2006) Experimental constraints on quaternary structure in Alzheimer's beta-amyloid fibrils. *Biochemistry* 45:498–512.
11. Fandrich M, Meinhardt J, Grigorieff N (2009) Structural polymorphism of Alzheimer Abeta and other amyloid fibrils. *Prion* 3:89–93.
12. Goldsbury CS, et al. (2000) Studies on the in vitro assembly of a beta 1–40: Implications for the search for a beta fibril formation inhibitors. *J Struct Biol* 130:217–231.
13. Meinhardt J, Sachse C, Hortschansky P, Grigorieff N, Fandrich M (2009) Abeta(1–40) fibril polymorphism implies diverse interaction patterns in amyloid fibrils. *J Mol Biol* 386:869–877.
14. Wetzel R, Shivaprasad S, Williams AD (2007) Plasticity of amyloid fibrils. *Biochemistry* 46:1–10.
15. Sachse C, et al. (2006) Quaternary structure of a mature amyloid fibril from Alzheimer's Abeta(1–40) peptide. *J Mol Biol* 362:347–354.
16. Sachse C, et al. (2007) High-resolution electron microscopy of helical specimens: A fresh look at tobacco mosaic virus. *J Mol Biol* 371:812–835.
17. Sachse C, Fandrich M, Grigorieff N (2008) Paired beta-sheet structure of an Abeta(1–40) amyloid fibril revealed by electron microscopy. *Proc Natl Acad Sci USA* 105:7462–7466.
18. Sawaya M, et al. (2007) Atomic structures of amyloid cross-beta spines reveal varied steric zippers. *Nature* 447:453–457.
19. Zandomeneghi G, Krebs MR, McCammon MG, Fandrich M (2004) FTIR reveals structural differences between native beta-sheet proteins and amyloid fibrils. *Protein Sci* 13:3314–3321.
20. Sunde M, et al. (1997) Common core structure of amyloid fibrils by synchrotron X-ray diffraction. *J Mol Biol* 273:729–739.
21. Bottcher B, Wynne SA, Crowther RA (1997) Determination of the fold of the core protein of hepatitis B virus by electron cryomicroscopy. *Nature* 386:88–91.
22. Jimenez JL, et al. (1999) Cryo-electron microscopy structure of an SH3 amyloid fibril and model of the molecular packing. *EMBO J* 18:815–821.
23. Tattum MH, et al. (2006) Elongated oligomers assemble into mammalian PrP amyloid fibrils. *J Mol Biol* 357:975–985.
24. Matthews BW (1968) Solvent content of protein crystals. *J Mol Biol* 33:491–497.
25. Diaz-Avalos R, King CY, Wall J, Simon M, Caspar DL (2005) Strain-specific morphologies of yeast prion amyloid fibrils. *Proc Natl Acad Sci USA* 102:10165–10170.
26. Antzutkin ON, Leapman RD, Balbach JJ, Tycko R (2002) Supramolecular structural constraints on Alzheimer's beta-amyloid fibrils from electron microscopy and solid-state nuclear magnetic resonance. *Biochemistry* 41:15436–15450.
27. Goldsbury C, Frey P, Olivieri V, Aebi U, Muller SA (2005) Multiple assembly pathways underlie amyloid-beta fibril polymorphisms. *J Mol Biol* 352:282–298.
28. Petkova A, et al. (2005) Self-propagating, molecular-level polymorphism in Alzheimer's beta-amyloid fibrils. *Science* 307:262–265.
29. Torok M, et al. (2002) Structural and dynamic features of Alzheimer's Abeta peptide in amyloid fibrils studied by site-directed spin labeling. *J Biol Chem* 277:40810–40815.
30. Zhang R, et al. (2009) Interprotofilament interactions between Alzheimer's Abeta1–42 peptides in amyloid fibrils revealed by cryoEM. *Proc Natl Acad Sci USA* 106:4653–4658.
31. Radford SE, Gosal WS, Platt GW (2005) Towards an understanding of the structural molecular mechanism of beta(2)-microglobulin amyloid formation in vitro. *Biochim Biophys Acta* 1753:51–63.
32. Sato T, et al. (2006) Inhibitors of amyloid toxicity based on beta-sheet packing of Abeta40 and Abeta42. *Biochemistry* 45:5503–5516.
33. Guo JT, Xu Y (2006) Amyloid fibril structure modeling using protein threading and molecular dynamics simulations. *Methods Enzymol* 412:300–314.
34. Olofsson A, Sauer-Eriksson AE, Ohman A (2006) The solvent protection of alzheimer amyloid-beta-(1–42) fibrils as determined by solution NMR spectroscopy. *J Biol Chem* 281:477–483.
35. Wall JS, Simon MN (2001) Scanning transmission electron microscopy of DNA-protein complexes. *Methods Mol Biol* 148:589–601.
36. Ludtke SJ, Baldwin PR, Chiu W (1999) EMAN: Semiautomated software for high-resolution single-particle reconstructions. *J Struct Biol* 128:82–97.
37. Frank J, et al. (1996) SPIDER and WEB: Processing and visualization of images in 3D electron microscopy and related fields. *J Struct Biol* 116:190–199.
38. Mindell JA, Grigorieff N (2003) Accurate determination of local defocus and specimen tilt in electron microscopy. *J Struct Biol* 142:334–347.

Supporting Information

Schmidt et al. 10.1073/pnas.0905007106

SI Materials and Methods

Congo Red Staining and Polarizing Microscopy. Aβ(1–42) fibrils were harvested in a BECKMAN Optima TLX ultracentrifuge (TLA 120.2 rotor, 30 min, 100,000 rpm, 20 °C). The pellet was soaked for 10 min in solution 1 before it was stained for 20 min with solution 2. The stained pellet was dehydrated by incubation in an ethanol series (80, 96, ≈100%). The incubation time for each ethanol step was 2 min. Afterward, stained fibrils were streaked out on a glass slide, embedded and analyzed with a NIKON 80i microscope, equipped with a polarizer and a DS-2Mv digital camera. Solution 1: 30 g of NaCl were added to 1 L of 80% ethanol and incubated for at least 24 h. Immediately before use, this solution was supplemented with 10 mL of a 1% NaOH stock solution. Solution 2: 5 g of Congo red and 30 g of NaCl were added to 1 L of 80% ethanol and incubated for at least 24 h. This solution was filtered, and immediately before use, 100 mL from this solution were supplemented with 1 mL from a 1% NaOH stock solution. Solutions 1 and 2 were used within 4 days.

Thioflavin-T Fluorescence Spectroscopy. All samples were recorded in 50 mM Tris/HCl buffer (pH 7.4). Final Aβ(1–42) peptide or Aβ(1–42) fibril concentrations were 0.05 mg/mL, and the thioflavin-T concentration was always 20 μM. All fluorescence measurements were carried out at room temperature and by using a SHIMADZU RF-5301PC fluorimeter (SHIMADZU). Emission spectra were recorded between 460 nm and 600 nm (emission slit setting 5), while exciting at 450 nm (emission slit setting 3).

Attenuated-Total Reflectance Fourier-Transform Infrared (ATR-FTIR) Spectroscopy. Infrared spectra were recorded using a BRUKER Tensor 27 spectrometer (BRUKER Optik) equipped with a BIO-ATR II cell and a LN-MCT Photovoltaic detector. Spectra represent the sum of 40 scans after reference subtraction and one times zero-filling. They were recorded at room temperature and at a resolution of 4 cm^{-1}. The analyzed fibril sample contained 2 mg/mL peptide in pure water. The pH was adjusted with NaOH to pH 7.4.

X-Ray Fiber Diffraction. Fibrils (lot 1010533) were grown at 5 mg/mL concentration. The solution was diluted with pure ethyleneglycol to a final ethyleneglycol concentration of 30 (vol/vol) %. Fibrils were harvested by centrifugation in a TLA-100 rotor (100,000 rpm, 30 min, 10 °C) using an Optima TLX centrifuge. An aliquot of the pellet was mounted on a 400 μM MicroMount loop (MiTeGen). The cryofrozen specimen was examined within a MicroMax 007 rotating anode generator (Cu, wavelength 1.5418 Å), equipped with a Saturn 944+ CCD detector and a XSTREAM 2000 system (Rigaku).

Platinum Side Shadowing. For platinum shadowing a Philips EM 400 T microscope was used. The fibrils were unidirectionally shadowed with platinum-iridium mixtures using elevation angles of 20° to 35° as described by Sachse C, et al. [(2006) Quaternary structure of a mature amyloid fibril from Alzheimer's Abeta(1–40) peptide. *J Mol Biol* 362:347–354.]

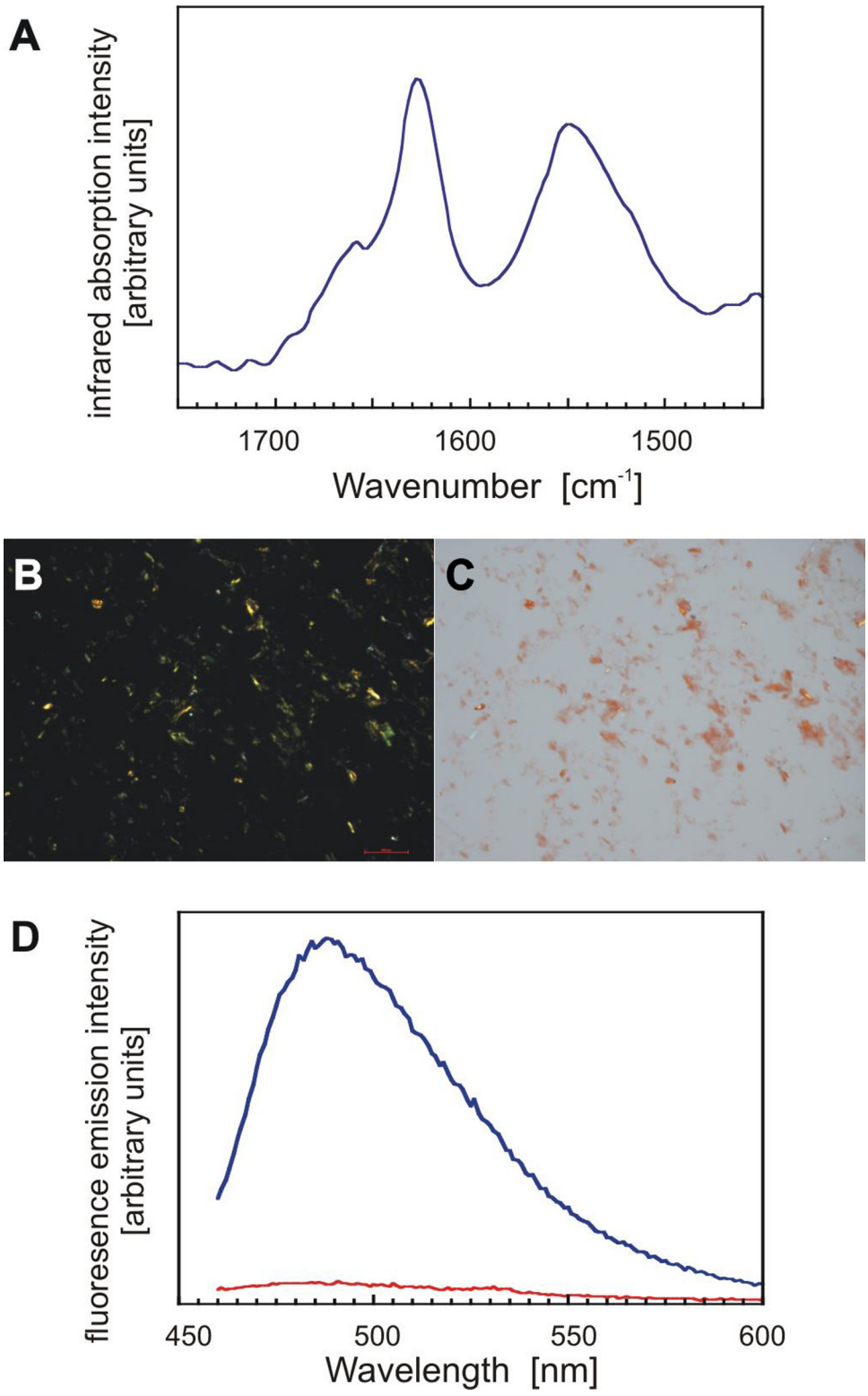

Fig. S1. Amyloid characteristics of the analyzed Aβ(1–42) fibrils. (*A*) ATR-FTIR spectrum of Aβ(1–42) fibrils. (*B*) Dark field and (*C*) bright field polarizing microscopy images of Congo red stained Aβ(1–42) fibrils showing green birefringence. (*D*) ThT fluorescence spectrum with (blue) or without (red) Aβ(1–42) fibrils.

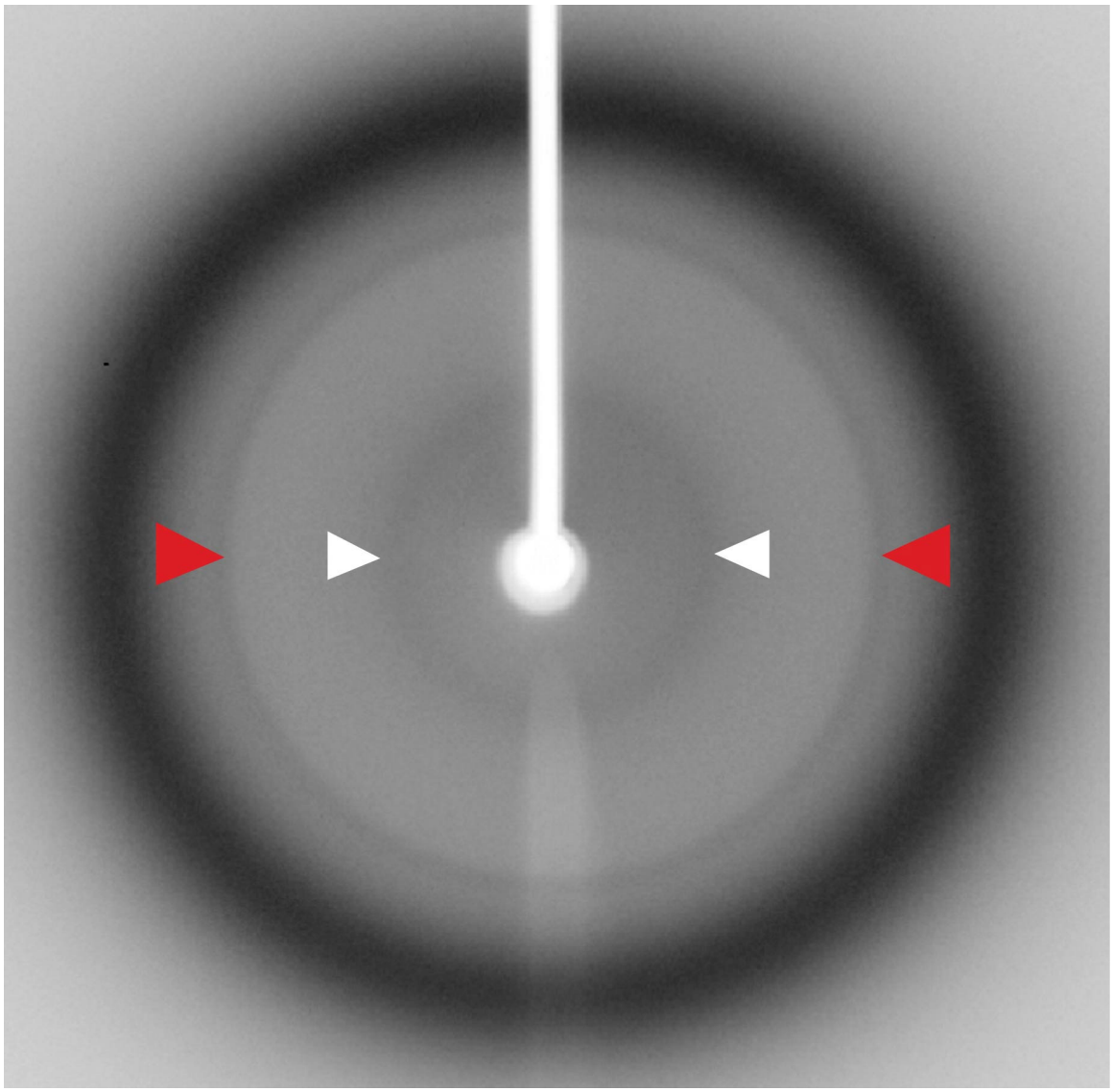

Fig. S2. X-ray diffraction image of fibrils cryofrozen in buffer and 30% ethylene glycol. White arrow heads: side chain spacing (9.7 ± 0.3 Å); red arrow heads: main chain spacing (4.67 ± 0.04 Å). Dark outer rim represents water scattering.

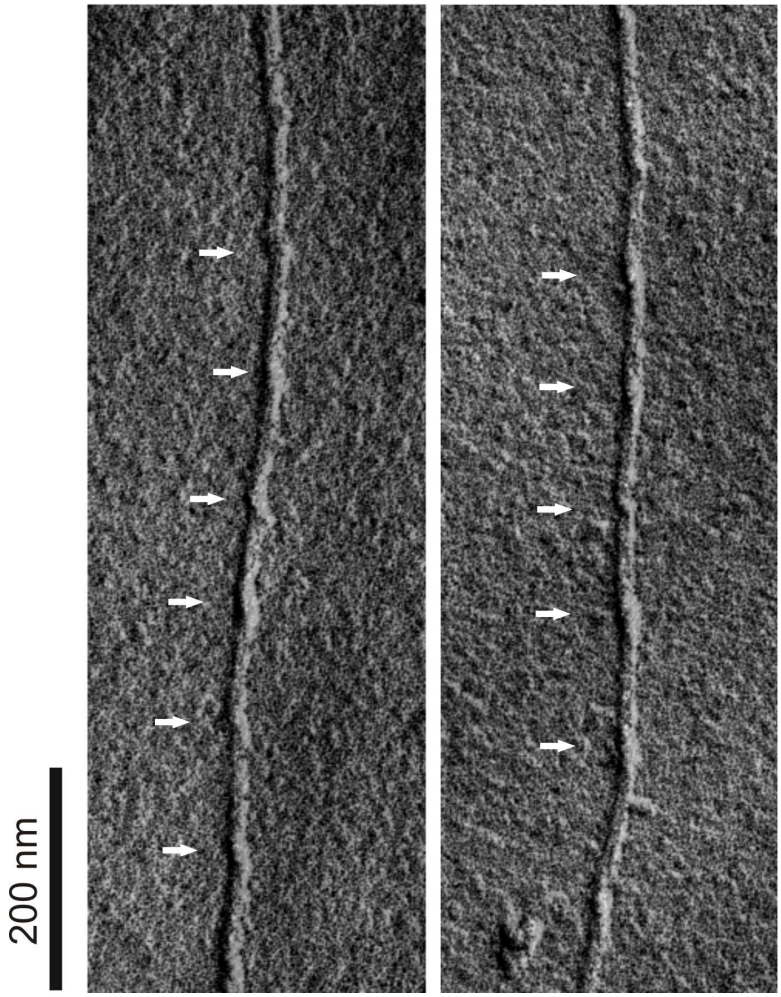

Fig. S3. Platinum side shadowing reveals left-hand fibril twist. White arrows show cross-over.

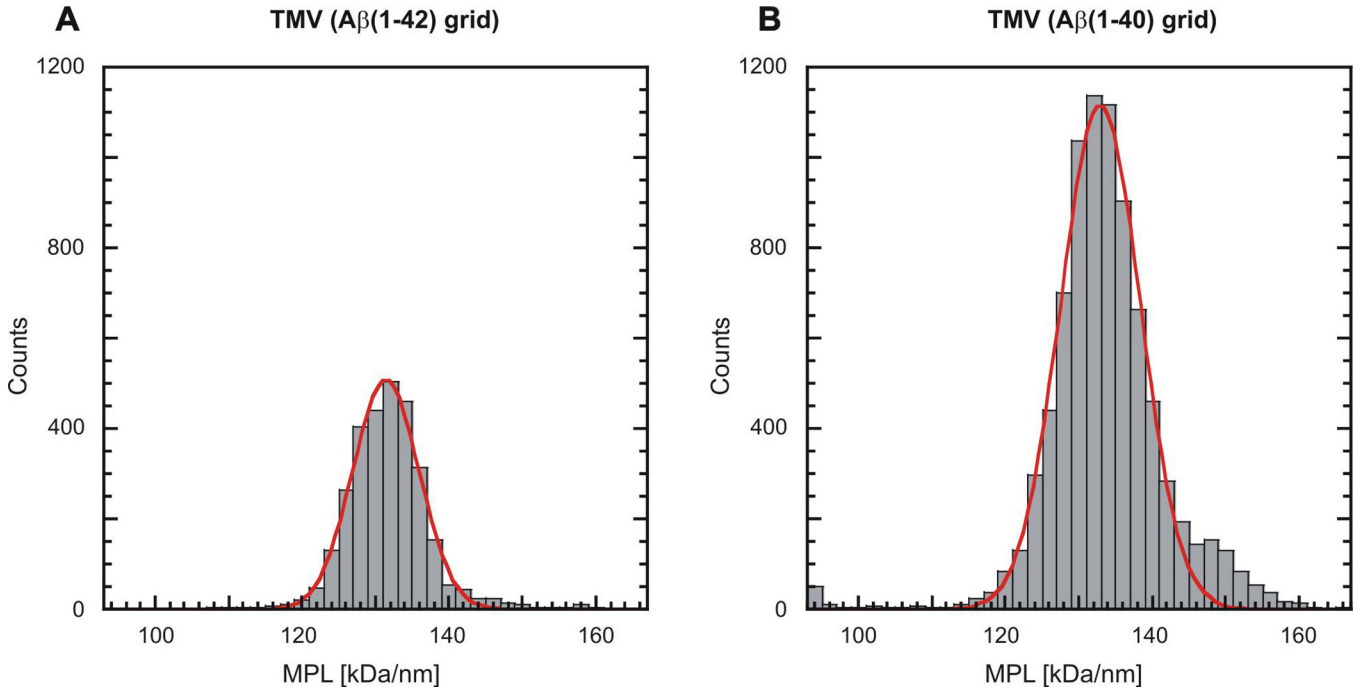

Fig. S4. Mass-per-length (MPL) measurements of TMV. (*A*) Histogram of MPL measurements of TMV used for calibration of grids containing Aβ(1–42) fibrils. The distribution has a standard deviation of 4.5 kDa/nm and the peak of the Gaussian fit occurs at 131.40 kDa/nm. The error of the peak position (standard deviation of the histogram divided by the square root of number of measurements) is 0.08 kDa/nm. (*B*) Same as *A* but for grids containing 20-nm and 13-nm Aβ(1–40) fibrils. The distribution has a standard deviation of 5.3 kDa/nm and the peak of the Gaussian fit occurs at 131.82 kDa/nm. The error of the peak position is 0.10 kDa/nm.

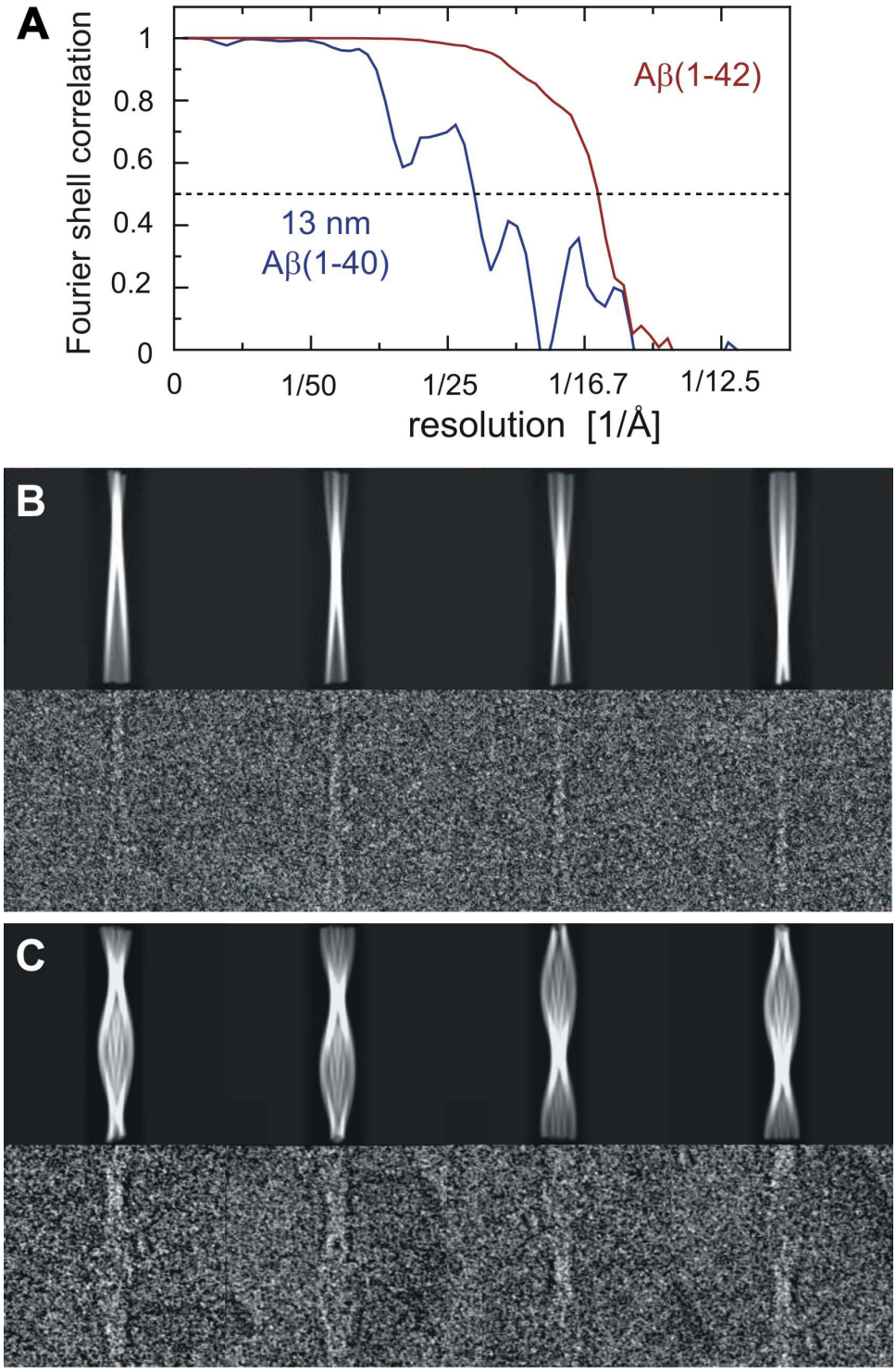

Fig. S5. Resolution of the reconstructed density and comparison with raw data. (*A*) FSC curve of the Aβ(1–42) fibril (red, FSC at 0.5 = 15 Å) and 13-nm Aβ(1–40) fibril (dark blue, FSC at 0.5 = 23 Å). (*B*) Comparison of raw cryo-EM images of Aβ(1–42) fibrils and projections from the reconstructed density show good correspondence. (*C*) Same as *B* but for the 13-nm Aβ(1–40) fibril.

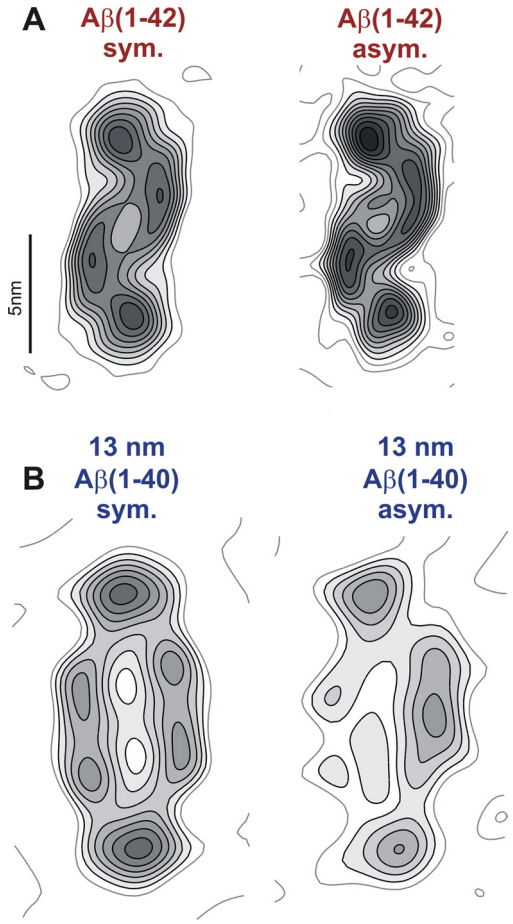

Fig. S6. Comparison of the cross-sectional density with and without imposing twofold symmetry. (*A*) Aβ(1–42) fibrils cross-section with and without imposed twofold symmetry. (*B*) 13-nm Aβ(1–40) fibrils cross-section with and without imposed twofold symmetry. The latter suffers substantially from noise, due to the small size of the dataset.